Separation Science and Technology
Publication details, including instructions for authors and subscription information:
http://www.informaworld.com/smpp/title~content=t713708471

Thermogravitational Field-Flow Fractionation: An Elution Thermogravitational Column

J. Calvin Giddings[a]; Michel Martin[a]; Marcus N. Myers[a]
[a] DEPARTMENT OF CHEMISTRY, UNIVERSITY OF UTAH, SALT LAKE CITY, UTAH

To cite this Article Giddings, J. Calvin , Martin, Michel and Myers, Marcus N.(1979) 'Thermogravitational Field-Flow Fractionation: An Elution Thermogravitational Column', Separation Science and Technology, 14: 7, 611 — 643
To link to this Article: DOI: 10.1080/01496397908057159
URL: http://dx.doi.org/10.1080/01496397908057159

SEPARATION SCIENCE AND TECHNOLOGY, 14(7), pp. 611–643, 1979

Thermogravitational Field-Flow Fractionation: An Elution Thermogravitational Column

J. CALVIN GIDDINGS, MICHEL MARTIN, and MARCUS N. MYERS

DEPARTMENT OF CHEMISTRY
UNIVERSITY OF UTAH
SALT LAKE CITY, UTAH 84112

Abstract

The major operating characteristics of thermal field-flow fractionation (thermal FFF) and of thermogravitational columns are compared, and it is shown that the two approaches can be advantageously combined in a method we call thermogravitational FFF. The theory of this technique is developed, with primary attention given to a change in the velocity profile under different flow conditions and its effect on component retention, column efficiency, resolution, and selectivity. Experimental results are shown to be in good overall accord with theory. It is shown that the potential of thermogravitational FFF lies in the fractionation of low molecular weight polymers or of other species having weak thermal diffusion.

INTRODUCTION

Field-flow fractionation (FFF) is an analytical separation technique whose concept was developed in 1966 (*1*). In FFF, separation is achieved by means of a lateral external field or gradient which interacts with solutes and forces them into different average velocity regimes within a long flow channel (*2*). Thermal field-flow fractionation (thermal FFF) is one of several subclasses of this technique. In thermal FFF the external "field" is a temperature gradient established in a channel confined between two parallel plates held at different temperatures. While other forms of FFF have been found applicable to a wide range of macromolecules and

particles, thermal FFF has been limited to the fractionation of synthetic polymers. The methodology and characteristics of thermal FFF in polymer studies have been described in earlier papers (*3–9*).

Normally, the metal plates of a thermal FFF system are oriented horizontally. The hot plate is placed on top and the cold plate on the bottom in order to assure stability against thermal convection. The thermal diffusion phenomenon forces polymers toward one wall of the channel—normally the cold wall—where they soon form a steady-state layer due to the opposing motion of diffusion. At the high dilutions approached by most analytical systems, the diffusion coefficient and the velocity induced by the thermal gradient can both be considered constant, and the resulting steady-state layer for each species is exponential in form (*2*). Increases in the temperature gradient compress the layer more tightly against the wall, increasing retention. In this way, gradient strength can be adjusted to yield optimum retention.

The compression of solute layers is greatest for the highest molecular weight components of the polymer mixture. These components, accordingly, accumulate preferentially in the near-stagnant fluid next to the wall where downstream motion is slight. Low molecular weight components, on the other hand, are subject to less compression because of weaker thermal diffusion effects and tend to form layers extending further into the high flow lamina of the channel where they are subject to a more rapid axial displacement. Fractionation therefore develops as a consequence of a coupled, field-flow induced, differential migration process along the channel. Theoretically, any number of components can be separated and eluted from a single thermal FFF channel. In practice, a programmed temperature gradient system is useful if one hopes to cover a wide range of molecular weights. Such a system has been applied successfully to polystyrene polymers ranging in molecular weight from 4000 to 7,100,000 (*7*).

The thermogravitational column is a much earlier device. This method, developed in 1938 by Clusius and Dickel (*10*), has been applied primarily to binary isotope mixtures. Like thermal FFF, the thermogravitational column utilizes thermal diffusion as the basic displacement step for separation. However, in the thermogravitational system the column must be oriented vertically, or at least have a vertical component. The lateral temperature gradient then has a horizontal component and this results in a horizontal density gradient. The latter causes an upward flow at the hot wall and a corresponding downward flow at the cold wall of the channel. This free or natural convective flow, which is countercurrent in nature,

occurs instead of the forced, unidirectional flow of FFF. The convective flow coupled with the thermal diffusion effect causes a cumulative separation effect along the length of the channel and allows much better enrichment than a single thermal diffusion cell. The highly enriched components eventually appear at the bottom and the top of the column. Since the thermogravitational column lacks a unidirectional flow component, it is not very well suited to the separation of multicomponent mixtures but is largely limited to binary systems. A review of the applications of the thermogravitational method has recently been published (*11*).

In this paper we demonstrate the combination of the thermogravitational method with field-flow fractionation. Basically, this is achieved by turning a thermal FFF channel on end so that its axis is vertical. One then gets the convective flow of the thermogravitational system superimposed on the forced flow of FFF. The unidirectional nature of the forced flow makes possible a continual elution of solute peaks and thus the separation of multicomponent mixtures.

While the addition of forced flow provides an obvious advance in versatility over the purely convective flow of the thermogravitational column, it is less obvious how convective flow contributes to the normal efficacy of forced flow thermal FFF. While this matter will be discussed in more detail later, we present here one important advantage of thermogravitational FFF over thermal FFF. We note first that separation in all forms of FFF is intricately involved with the flow profile in the channel. Unfortunately, these profiles are subject to little control or variation. In the usual (ribbonlike) parallel plate channels the profile is normally parabolic, although small deviations from this are experienced as a result of changes in viscosity with temperature over the channel width in thermal FFF. However, in thermogravitational FFF the flow profile is the sum of two quite unlike component profiles whose relative contributions can be varied as desired. Thus the thermogravitational FFF column provides a means of gaining some control over flow profiles in FFF methodology, thereby potentially improving separations. We will discuss some detailed aspects of this new measure of control in subsequent sections of this paper.

THEORY

Channel Velocity Profile

In slow laminar fluid motion, flow velocities are linear in the forces inducing the flow. When forces are doubled, the velocity at each point

likewise doubles. Because forces are additive, two or more different sets of forces acting on a fluid will yield a flow profile equal to the sum of the individual profiles for the force sets acting separately. In thermogravitational FFF, where both external pumping forces and internal convective forces (originating in density differences) exist simultaneously, the channel velocity profile is the sum of the two component profiles. Each of the two component flows has been analyzed extensively in studies of thermal FFF and thermogravitational columns, respectively. We consider the latter first.

Analysis of temperature and velocity profiles in thermogravitational columns have been presented by Elder (*12*). The velocity pattern was found to be dependent on the Rayleigh number, A,

$$A = \gamma' g \rho \Delta T w^3 / \kappa \eta \tag{1}$$

where γ' is the coefficient of thermal expansion of the fluid, ρ the density, κ the thermal diffusivity (equal to $\lambda'/\rho c_p$, λ' being the thermal conductivity and c_p the specific heat at constant pressure), η the viscosity, g the gravitational acceleration, and ΔT the temperature difference between the parallel plates separated by a distance w. When A is smaller than 10^3, a stable unicellular circulation is generated and the flow is vertical throughout the channel except for regions within a distance on the order of w from the ends. Furthermore, under these conditions ($A < 10^3$), the temperature profile in the channel is linear (*13*).

We expect thermogravitational FFF to normally satisfy the criterion $A < 10^3$. For instance, for the present study, using ethylbenzene as a solvent with a temperature drop of 40 °C between the plates and a channel thickness of 0.127 mm, the Rayleigh number is calculated to be 16.7 if one takes for the temperature-dependent variables their values at 38 °C, which is the temperature at the center of the channel (*14*). Even if ΔT and w are both doubled, A is still well removed from 10^3 and unicellular convection flow is expected to persist. The flow profile existing under these circumstances is given by the following expression in which the upward velocities are positive (*15–21*):

$$v_{\text{free}}(x) = -\frac{\bar{\rho}\gamma' g w^2 \Delta T}{12\eta} \frac{x}{w}\left(1 - \frac{x}{w}\right)\left(1 - \frac{2x}{w}\right) \tag{2}$$

where $\bar{\rho}$ is the average density in the channel and x is the distance from the cold wall. This profile is shown as the bottom curve in Fig. 1.

Equation (2) is based on the assumption that γ' and η do not depend on the temperature and on the variation of the composition of the liquid

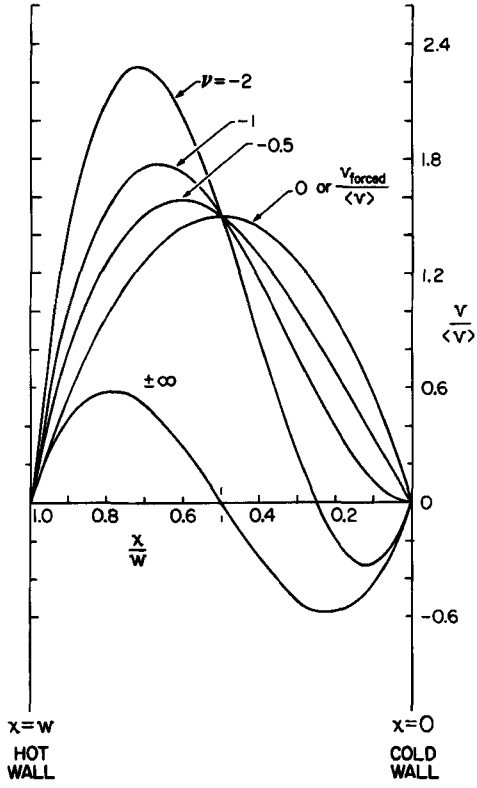

FIG. 1. Velocity profiles in thermogravitational FFF channels for free convection flow ($\nu = \pm\infty$), forced flow ($\nu = 0$), and various composite flows ($\nu = -0.5, -1, -2$).

in the channel. In most analytical applications of thermogravitational FFF, solute concentrations may be assumed so low that compositional variations are negligible. Temperature-dependent effects, while not always negligible, are generally small. The temperature dependence of γ', for example, is generally slight in the temperature range of FFF operation. However, the temperature dependence of viscosity is often larger. For instance, the viscosity of ethylbenzene falls roughly twofold from 20 to 80°C. Even so, it has been shown that a change in the viscosity by a factor of about 2 does not significantly change the velocity profile (*22*).

Equation (2) also assumes that the temperature gradient in the channel

is constant, which requires that the thermal conductivity of the solvent be constant. This has been shown to be a reasonable approximation (*23*).

The velocity profile due to forced flow in the channel between two infinite parallel plates is parabolic:

$$v_{\text{forced}}(x) = 6\langle v\rangle(x/w)(1 - x/w) \tag{3}$$

where $\langle v\rangle$ is the average velocity in the channel. This equation is also based on a constant viscosity of the liquid across the channel. The perturbations of the profile due to the temperature dependence of viscosity have been studied recently (*24*). As the disturbances are relatively small, and because we do not have similar corrections for this effect with the free convection profile, we shall assume that Eq. (3) provides an adequate description of the velocity distribution for forced flow. The form of the resulting parabolic profile is shown in Fig. 1 by the curve identified with $v = 0$.

It is interesting to note that the positions of the two extremes of the free convection profile (at $x/w = 1/2 \pm \sqrt{3}/6$) are those for which the velocities of the forced flow profile equal the average velocity $\langle v\rangle$.

The final flow profile in the thermogravitational FFF channel is the sum of the profiles expressed by Eqs. (2) and (3):

$$v = -\frac{\delta\bar{\rho}\gamma' g w^2 \Delta T}{12\eta}\frac{x}{w}\left(1 - \frac{x}{w}\right)\left(1 - \frac{2x}{w}\right) + 6\langle v\rangle\frac{x}{w}\left(1 - \frac{x}{w}\right) \tag{4}$$

Because it is desirable to have forced flow always positive in this equation whether its direction is up or down, parameter δ must equal $+1$ for upward flow (the normal case) and -1 for downward forced flow.

We can simplify Eq. (4) by defining the terms

$$v_1 = -\delta\bar{\rho}\gamma' g w^2 \Delta T/12\eta \tag{5}$$

$$v_2 = 6\langle v\rangle \tag{6}$$

With these, the overall profile of Eq. (4) becomes

$$v = \frac{x}{w}\left(1 - \frac{x}{w}\right)\left[v_1\left(1 - \frac{2x}{w}\right) + v_2\right] \tag{7}$$

which, rearranged, assumes the form

$$v = (v_1 + v_2)\frac{x}{w} - (3v_1 + v_2)\left(\frac{x}{w}\right)^2 + 2v_1\left(\frac{x}{w}\right)^3 \tag{8}$$

It is convenient to introduce a dimensionless parameter, v, reflecting

the relative importance of the free and forced component flows

$$\nu = v_1/v_2 \tag{9}$$

or, with Eqs. (5) and (6),

$$\nu = -\delta\bar{\rho}\lambda' g w^2 \Delta T/72\eta\langle v\rangle \tag{10}$$

which shows that ν is positive for downward forced flow and negative for upward flow. With the introduction of ν the velocity profile becomes

$$v = 6\langle v\rangle[(1 + \nu)x/w - (1 + 3\nu)(x/w)^2 + 2\nu(x/w)^3] \tag{11}$$

By comparison with Eq. (3), it is clear that when $\nu = 0$ the flow becomes parabolic.

Flow profiles expressed as $v/\langle v\rangle$ are shown for various ν values in Fig. 1. As noted before, the flow is entirely of a forced nature when $\nu = 0$ and is totally free convective when $|\nu| = \infty$. For the latter curve, however, the profile has been renormalized because $v/\langle v\rangle$ goes to infinity. In this case we have simply plotted Eq. (2) with $(\bar{\rho}\gamma' g w^2 \Delta T/12\eta) = 6$.

While the composite flow profiles of Fig. 1 all correspond to negative ν values, one can readily envision positive ν values (downward forced flow) by turning the figure upside down, changing the sign of ν for each curve, and exchanging the labels for hot and cold walls.

Figure 1 and Eq. (7) show that the velocity can have a direction opposite to the average velocity over limited regions for which $\nu(1 - 2x/w) + 1 < 0$. This local reversal is only possible for $|\nu| > 1$. When a significant fraction of a solute is located in a velocity reversal region, one would expect unusual retention characteristics for this solute. Since polymers in a thermal field are concentrated in an exponential layer against the cold wall (*3*), such a situation can happen for upward flow of relative magnitude $\nu < -1$. Downward flow, on the other hand, offers no unusual retention characteristics for polymers collecting at the cold wall. This is why the experiments reported here operate with upward flow.

Retention

The mean velocity of solute zones in all variants of FFF is

$$\mathscr{V} = \langle cv\rangle/\langle c\rangle \tag{12}$$

where v, as before, is the local velocity of the carrier liquid and c the local concentration of solute. The $\langle\ \rangle$ brackets indicate cross-sectional averages.

The solute concentration profile in thermal FFF is obtained as a solution of the following differential equation (*3*):

$$\frac{d \ln c}{dx} = -\left(\frac{\alpha}{T} + \gamma'\right)\frac{dT}{dx} = -\frac{1}{\ell} \tag{13}$$

where α is the thermal diffusion factor of the solute. If one assumes that ℓ is constant, a direct integration of Eq. (13) yields

$$c = c_0 \exp(-x/\ell) = c_0 \exp(-x/\lambda w) \tag{14}$$

where c_0 is the concentration of solute at the cold wall. Quantity ℓ represents the mean "thickness" of the solute zone and λ is a fundamental dimensionless parameter, ℓ/w, characteristic of the zone.

The retention ratio R, which expresses the zone velocity $\mathscr{V}$ relative to the mean carrier velocity $\langle v \rangle$, is given by

$$R = \frac{\mathscr{V}}{\langle v \rangle} = \frac{\langle cv \rangle}{\langle c \rangle \langle v \rangle} \tag{15}$$

By combining Eqs. (11), (14), and (15), and working out the averages of the latter, we obtain R which, as a function of λ and v, becomes

$$R = 6\lambda v(1 - R_p) + R_p \tag{16}$$

where R_p is the retention ratio obtained for parabolic flow, $v = 0$, and is given by the classical FFF equation

$$R_p = 6\lambda \mathscr{L}(1/2\lambda) \tag{17}$$

where $\mathscr{L}(y)$ is the Langevin function

$$\mathscr{L}(y) = \coth y - 1/y \tag{18}$$

The contributions to R from the individual flow components can be distinguished in Eq. (16): R_p for the forced flow and $6\lambda v(1 - R_p)$ for the free convection. While R_p always lies between zero and unity (*2*) whether or not R is greater or smaller than R_p or even outside the range 0–1, it depends on the sign of v and the magnitude of the associated terms. Thus $R > R_p$ for downward flow (v positive) and $R < R_p$ for upward flow (v negative). The inequalities arise from the fact that the solute zone is most concentrated near the cold wall, and thus the perturbation of the flow due to free convection near this wall is crucial. For downward flow the total velocity near the cold wall is greater than the velocity due to parabolic flow alone, giving $R > R_p$. For upward flow, as is clear from Fig. 1, velocity reversal occurs near the cold wall for $v < -1$, and solute can

then be carried in a direction opposite to the forced flow. In this case, R becomes negative. In less extreme cases R may equal zero (forming stationary zones), or, if positive, $R < R_p$ in all cases.

The above features are illustrated in Fig. 2 where plots of R versus λ are shown for different ν values. These curves can be compared with the normal parabolic FFF curve ($\nu = 0$).

The limiting forms of the retention expressions, Eqs. (16) through (18), are obtained as

$$\lim_{\lambda \to 0} R = 6\lambda(1 + \nu) - 12\lambda^2(1 + 3\nu) \tag{19}$$

$$\lim_{\lambda \to \infty} R = 1 + \frac{\nu}{10\lambda} - \frac{1}{60\lambda^2} - \frac{\nu}{420\lambda^3} \tag{20}$$

In the special case $\nu = -1$, the two individual velocity components exactly cancel each other at the cold wall (see Fig. 1), thus eliminating the

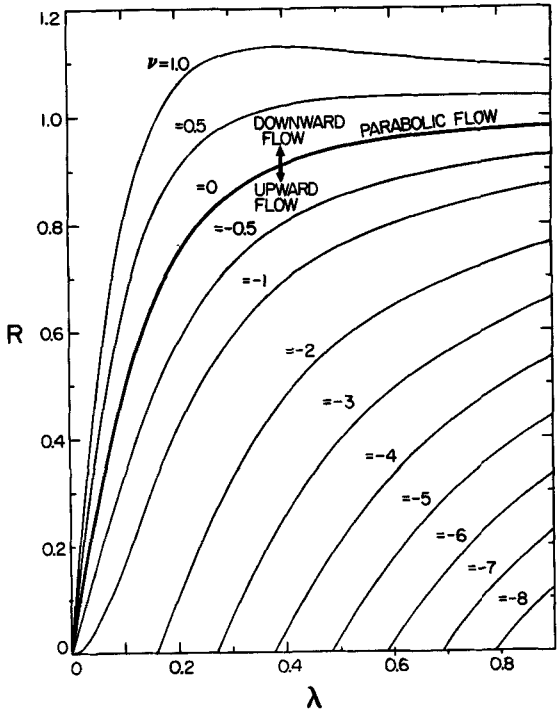

FIG. 2. Retention ratio R vs λ for different ν values, according to Eq. (16).

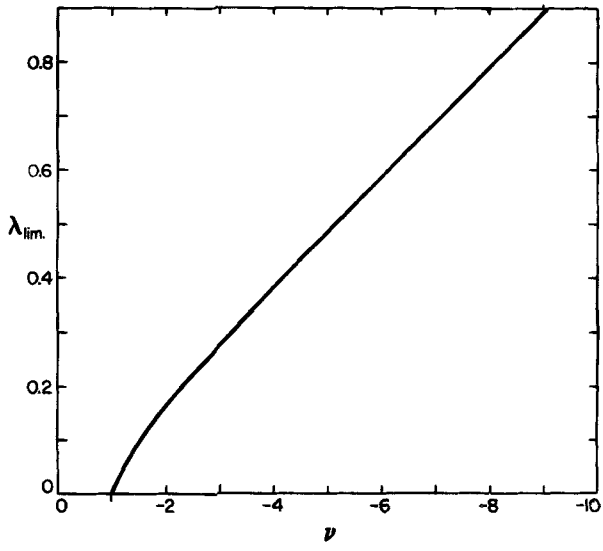

FIG. 3. Plot of λ_{lim} (value of λ for which $R = 0$) vs ν.

linear term in λ from Eq. (19). We find

$$\lim_{\lambda \to 0} R(\nu = -1) = 24\lambda^2 - 72\lambda^3 \tag{21}$$

It must be noted that when $\nu < -1$, the limiting value of R when $\lambda \to 0$ is negative. However, as λ increases above zero, a limiting value is reached, λ_{lim}, at which R turns positive. This value is a solution of the following equation:

$$\mathcal{L}(1/2\lambda_{lim}) = \nu/(6\lambda_{lim}\nu - 1) \tag{22}$$

and is plotted against ν in Fig. 3. In the range $-3 > \nu > -10$, λ_{lim} is given within 1% accuracy by the empirical relationship

$$\lambda_{lim} = -0.02784 - 0.10229\nu \tag{23}$$

Column Efficiency

There are several processes that contribute to peak broadening during solute migration in the FFF channel. These have been recently reviewed (*8*). All are affected in some way by the velocity distribution in the channel. The longitudinal molecular diffusion contribution to the plate height H

is given by

$$H_D = 2D/R\langle v\rangle \tag{24}$$

and can be estimated by using the R value in Eq. (16). However, because of the sluggish diffusion of polymers, this term is usually small, even for very low R values. Indeed, the diffusion coefficient D is approximately proportional to $M^{-0.55}$ where M is the molecular weight of the solute (*23*), while R from Eq. (19) varies roughly as $6\lambda(1 + v)$, where λ is approximately (*4*)

$$\lambda = \phi/\Delta T M^{0.5} \tag{25}$$

Therefore, R is proportional to $M^{-0.5}$. Consequently H_D is nearly independent of M, and thus of R. Some exceptions to this rule occur for $v = -1$ and $v < -1$, but in almost all cases the contribution of H_D remains negligible and need not be discussed further.

The most important contribution to peak broadening in FFF originates in the nonequilibrium phenomenon, which is due to the fact that molecules in different streamlines travel at different velocities, thus upsetting the equilibrium concentration distribution and causing axial zone broadening. The contribution to H is usually expressed in one of two forms:

$$H_N = \chi w^2\langle v\rangle/D \tag{26}$$

$$= \psi \ell^2 \mathscr{V}/D \tag{27}$$

where the coefficients χ and ψ are complicated functions of λ and v of the from (*25*)

$$\psi = 2F/R^2(1 - e^{-1/\lambda}) \tag{28}$$

$$\chi = 2\lambda^2 F/R(1 - e^{-1/\lambda}) \tag{29}$$

in which

$$\begin{aligned} F = {} & 2A[6(1 + v) - (A + 1)/\lambda + 36v\lambda^2 \\ & - 6\lambda(1 + 6v) + 18\lambda e^{-1/\lambda}(1 - 10v\lambda)] \\ & + 72\lambda^2[(1 + v)^2 - 10(1 + 4v + 3v^2)\lambda \\ & + 4(7 + 69v + 90v^2)\lambda^2 - 672v(1 + 3v)\lambda^3 + 4464v^2\lambda^4] \\ & - 72\lambda^2 e^{-1/\lambda}[(7 - 2v + v^2) + 2(5 - 68v + 15v^2)\lambda \\ & + 4(7 - 69v + 180v^2)\lambda^2 - 672v(1 - 3v)\lambda^3 + 4464v^2\lambda^4] \end{aligned} \tag{30}$$

and where the term A is

$$A = 12\lambda e^{-1/\lambda}(6v\lambda - 1)/(1 - e^{-1/\lambda}) \tag{31}$$

In Figs. 4 and 5, ψ is plotted versus λ for positive and negative values of v, respectively. When v is smaller than -1, the curves approach infinity from both sides of the λ value for which R is zero. This is physically reasonable because plate height, which is the ratio of peak variance to migration distance, is expected to approach infinity when migration ceases ($R = 0$). Similar results are expected for the χ curves, which are plotted in Figs. 6 and 7. Here the plots are actually of $|\chi|$, since χ is negative for low λ values when $v < -1$ because the direction of motion of the peak is negative.

The limiting expressions for χ and ψ for high and low retention are (*25*)

$$\lim_{\lambda \to 0} \psi \ (v \neq -1) = 4[1 - 6(1 + 3v)\lambda/(1 + v) + 84v\lambda^2/(1 + v)] \tag{32}$$

$$\lim_{\lambda \to 0} \psi \ (v = -1) = 28[1 - 6\lambda + (36/7)\lambda^2] \tag{33}$$

$$\lim_{\lambda \to 0} \chi \ (v \neq -1) = 24\lambda^3[(1 + v) - 8(1 + 3v)\lambda + 12(1 + 14v + 17v^2)\lambda^2/(1 + v)] \tag{34}$$

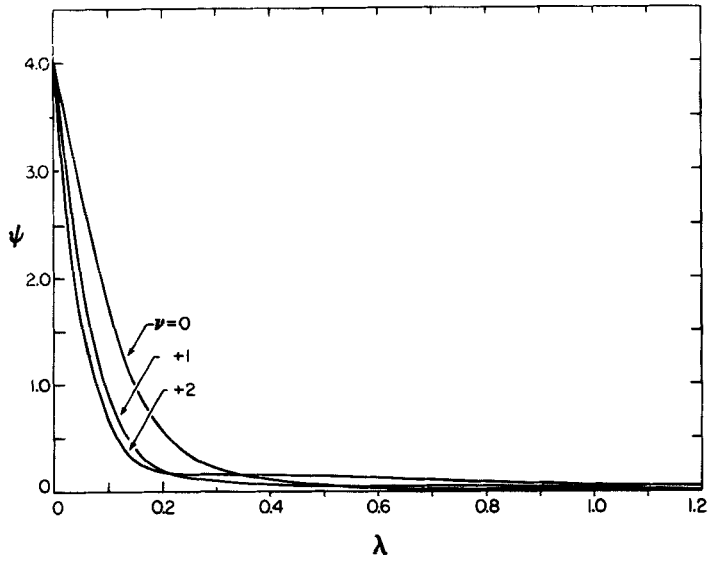

FIG. 4. ψ vs λ curves for thermogravitational FFF with downward flow.

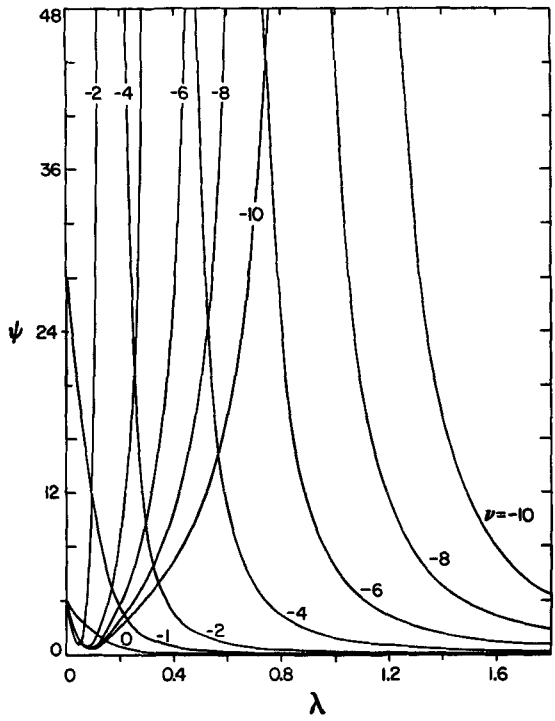

FIG. 5. ψ vs λ curves for thermogravitational FFF with upward flow.

$$\lim_{\lambda \to 0} \chi\,(v = -1) = 672\lambda^4[1 - 9\lambda + (90/7)\lambda^2] \tag{35}$$

$$\lim_{\lambda \to \infty} \chi = (1/105)(1 + 3v^2) \tag{36}$$

$$\lim_{\lambda \to \infty} \psi = 0 \tag{37}$$

We note that when $\lambda \to 0$, F in Eqs. (28) and (29) becomes equal to the second of the three terms in Eq. (30). This limit is valid to better than 2% for $\lambda < 0.1$. We note also that the limiting value of χ for low retention ($\lambda \to \infty$) does not depend on the sign of v, which results from the fact that solute becomes uniformly distributed across the thickness of the channel and is equivalently affected by upward and downward flow.

It is clear from Figs. 6 and 7 that when $|v| > 2$, the peak broadening parameter χ is much larger than it is for parabolic flow. This arises in the fact that for a given average flow, $\langle v \rangle$, the velocity variations are more

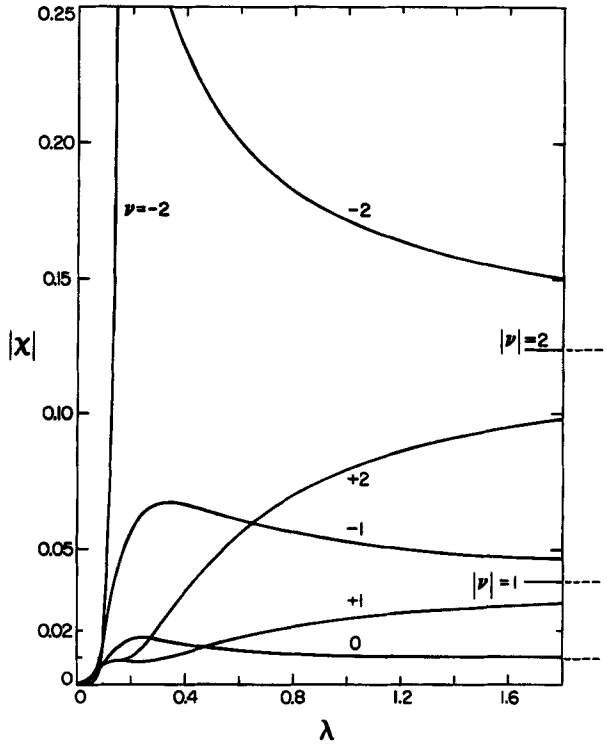

FIG. 6. $|\chi|$ vs λ curves for thermogravitational FFF with $|\nu| \leq 2$.

severe for a composite velocity profile than for a parabolic one. However, this is no longer true for solutes highly compressed near the cold wall because the latter will experience smaller relative velocity variations than they would under parabolic conditions.

Another phenomenon contributing to peak broadening in thermogravitational FFF is the relaxation effect. This refers to the uneven displacement of solute by the channel velocity profile in the short period between injection and the achievement of a steady-state distribution. Its contribution to the plate height is affected by the velocity distribution in the channel and hence by the value of ν. However, in the thin channel used in the present system, the relaxation time is very short in comparison with the elution time and, therefore, the relaxation effect can be neglected.

Another important contribution to H encountered with all high resolution systems applied to polymers is that due to polydispersity. While this

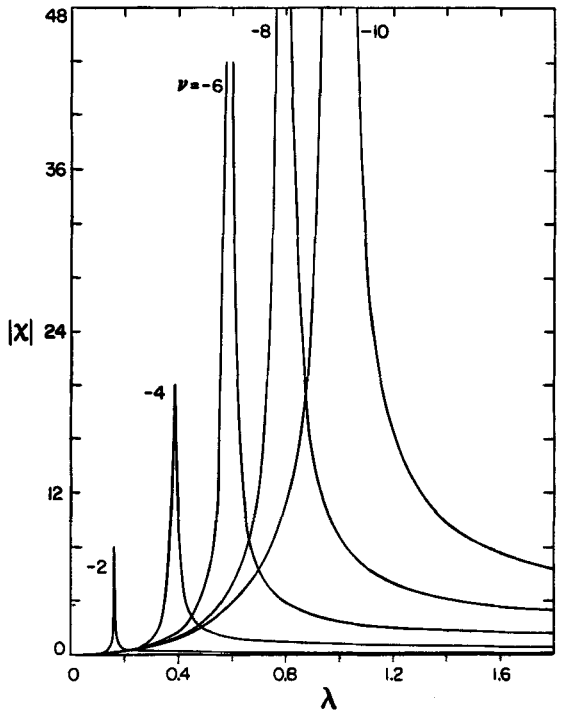

FIG. 7: $|\chi|$ vs λ curves for thermogravitational FFF with $\nu \leq -2$.

contribution is independent of the actual value of $\langle v \rangle$ (*3*), its analytical expression (*8*) contains the term $d \ln R/d \ln \lambda$, which depends on the form of $R(\lambda)$ and thus depends on ν (Eq. 16). The magnitude of the polydispersity contribution to the plate height depends on the extent of the disengagement of the unequal polymers of the sample; that is, on the ability of the system to separate close-lying species. As the phenomenon and the equations describing it are basically the same in thermogravitational FFF as in other FFF systems, we will omit detailed considerations (*3*, *8*).

Resolution and Selectivity

The resolution, R_s, of two components migrating in an FFF channel or even in a chromatographic column can be expressed by (*6*)

$$R_s = (\sqrt{N}/4)\Delta R/R \tag{38}$$

where N is the average number of theoretical plates for the components and $\Delta R/R$ is the relative difference in their retention ratio. For FFF systems this equation can be expressed in the alternate form (*9*)

$$R_s = \frac{\sqrt{N}}{4}\left|\frac{d \ln R}{d \ln \lambda}\right|\left|\frac{d \ln \lambda}{d \ln N}\right|\frac{\Delta M}{M} \tag{39}$$

where $\Delta M/M$ is the relative difference in the molecular weights of the two components and $|d \ln \lambda/d \ln M| = \gamma$ is a constant which according to Eq. (25) is 0.5 and according to some experimental evidence is closer to 0.6. We can write Eq. (38) in the general γ-containing form without, for the moment, specifying whether γ is closer to 0.5 or 0.6:

$$R_s = (\gamma\sqrt{N}/4)|d \ln R/d \ln \lambda|\Delta M/M \tag{40}$$

This equation shows that R_s depends on two factors: column efficiency, which is expressed by N, and selectivity, which is given by $\gamma|d \ln R/d \ln \lambda|$.

For the thermogravitational FFF system we use Eqs. (16) through (18) to obtain the selectivity term

$$\frac{d \ln R}{d \ln \lambda} = 1 - \frac{6v\lambda R_p}{R} + \frac{12\lambda(1 - 6v\lambda)}{R}\left[\frac{e^{-1/\lambda}}{\lambda(1 - e^{-1/\lambda})^2} - \lambda\right] \tag{41}$$

This term is plotted against λ in Fig. 8 using different v values. The limiting forms of the curves can be derived from Eqs. (19) through (21).

$$\lim_{\lambda \to 0} (d \ln R/d \ln \lambda) = 1 - 2\lambda(1 + 3v)/(1 + v), \qquad \text{for} \quad v \neq -1 \tag{42}$$

$$\lim_{\lambda \to 0} (d \ln R/d \ln \lambda) = 2 - 3\lambda, \qquad \text{for} \quad v = -1 \tag{43}$$

$$\lim_{\lambda \to \infty} (d \ln R/d \ln \lambda) = -(v/10\lambda) + (10 + 3v^2)/300\lambda^2 \tag{44}$$

Generally the curves of Fig. 8 show a continuous decrease in selectivity (and thus in resolution) for increasing values of λ. An exception is observed for positive values of v for which $d \ln R/d \ln \lambda$ goes to zero at a finite λ value. This arises because as λ increases, R passes through a maximum value which exceeds unity. At the maximum, selectivity is zero. On the side of the maximum for which R decreases with λ, the retention order is inverted and selectivity regains a finite level.

It is instructive to compare the curves of Fig. 8 corresponding to $v \neq 0$ with the one corresponding to parabolic flow ($v = 0$). A considerable enhancement in selectivity is observed for $v < 0$ compared to the parabolic case. When $v < -1$ and $\lambda = \lambda_{\text{lim}}$, which corresponds to $R = 0$, $d \ln R/$

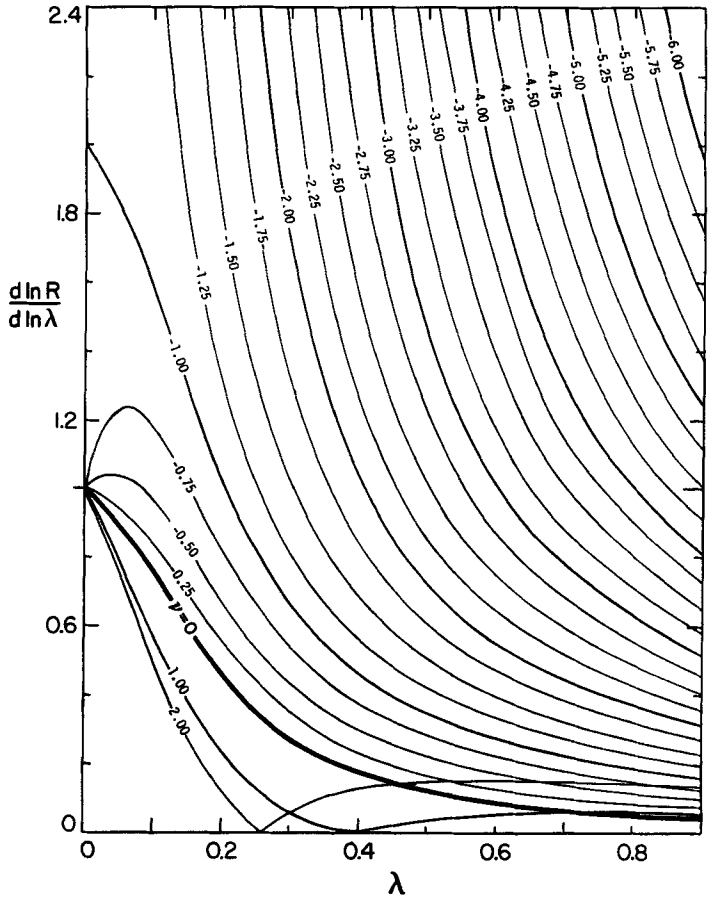

FIG. 8. Plots of the selectivity term, $|d \ln R/d \ln \lambda|$, as a function of λ for different values of ν.

$d \ln \lambda$ becomes infinite. This suggests that very high resolution can be achieved as one approaches these particular conditions.

Figure 8 shows, more generally, that the selectivity in the case of upward flow can be raised to any specified value by the proper adjustment of the parameter ν, since for $\nu < -1$ every curve has a vertical asymptote. This is particularly interesting for low molecular weight components (high λ values) for which the selectivity with normal parabolic flow is poor.

The enhanced selectivity of thermogravitational FFF is shown more explicitly in Fig. 9 where $d \log (V_r/V^0)/d \log M$ is plotted against $\log M$ for different ν values. Here V_r/V^0 is the retention volume divided by the void volume. It has been established that the resolution is related to the fractionating power, $(1/\theta) = M/\delta M$, where δM is the minimum increment in molecular weight separable at unit resolution (5). Quantity $1/\theta$ is given by

$$1/\theta = (\sqrt{N}/4)|d \log (V_r/V^0)/d \log M| \tag{45}$$

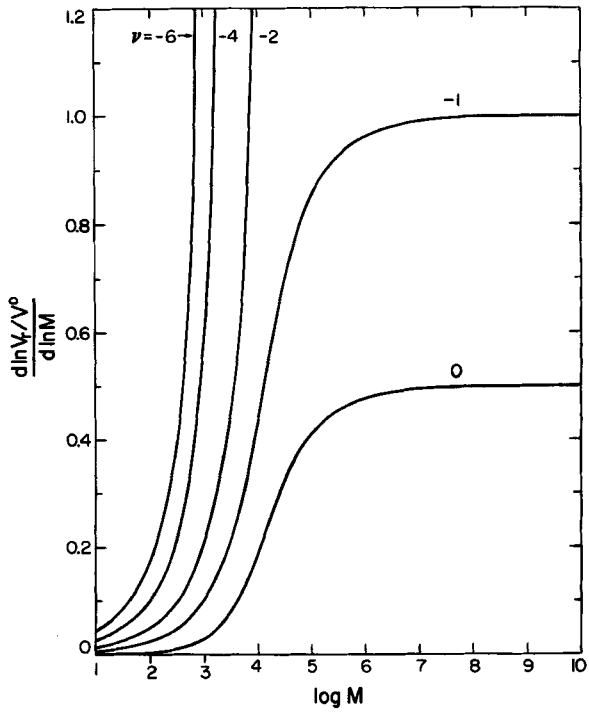

FIG. 9. Plot of selectivity, $d \ln (V_r/V^0)/d \ln M$, vs $\log M$ for thermogravitational FFF with upward flow. We use $M = 560/\lambda^2$ (see text).

The curves of Fig. 9 are related to those of Fig. 8 since

$$\left|\frac{d\log(V_r/V^0)}{d\log M}\right| = \left|\frac{d\ln R}{d\ln\lambda}\cdot\frac{d\ln\lambda}{d\ln M}\right| \tag{46}$$

Because $|d\ln\lambda/d\ln M| = \gamma$, Eq. (46) can be written

$$\left|\frac{d\log(V_r/V^0)}{d\log M}\right| = \gamma\left|\frac{d\ln R}{d\ln\lambda}\right| \tag{47}$$

For the plots of Fig. 9 the molecular weights are related to the λ values by Eq. (25) with $\phi = 1420°C\ (g/mole)^{1/2}$ (7) and $\Delta T = 60°C$. This gives $M = 560/\lambda^2$. The figure shows clearly that high values of $|d\log(V_r/V^0)/d\log M|$ can be obtained by properly choosing ν for molecular weights $> \sim 500$.

Figure 9 can also be used to compare the relative merits of thermogravitational FFF and a pressurized horizontal FFF system for separating low molecular weight components (6). Pressurizing the channel extends the liquid range of the solvent and thus allows the use of a greater ΔT and the realization of a smaller λ for any given species. Consequently, the curve for $\nu = 0$ is shifted left, bringing increased selectivity (up to ~ 0.5) to low molecular weight components. One can profitably vary ΔT in the thermogravitational system also, but by varying ν one can reach selectivity values considerably higher than the limiting value of $\gamma \sim 0.5$ even for the low molecular weight species.

Although selectivity considerations favor thermogravitational FFF over normal thermal FFF, the thermogravitational system tends to be less efficient than normal FFF. The combined effect of these two opposing influences is shown below.

If we substitute L/H (channel length over plate height) for the number N of theoretical plates in Eq. (40), we get

$$R_s = \frac{\gamma}{4}\sqrt{\frac{L}{H}}\left|\frac{d\ln R}{d\ln\lambda}\right|\frac{\Delta M}{M} \tag{48}$$

With the substitution of Eq. (26) for H this becomes

$$R_s = \left[\frac{\gamma}{4}\sqrt{\frac{LD}{w^2\langle v\rangle}}\frac{\Delta M}{M}\right]\sqrt{\frac{1}{\chi}}\left|\frac{d\ln R}{d\ln\lambda}\right| \tag{49}$$

where the terms in brackets are constant for a given channel (L, w), a given separation problem ($\Delta M/M$, D, γ), and a given average velocity $\langle v\rangle$. In the thermogravitational system, of course, $\langle v\rangle$ will affect ν and thus χ. The remaining terms, which include χ, form the crucial resolution

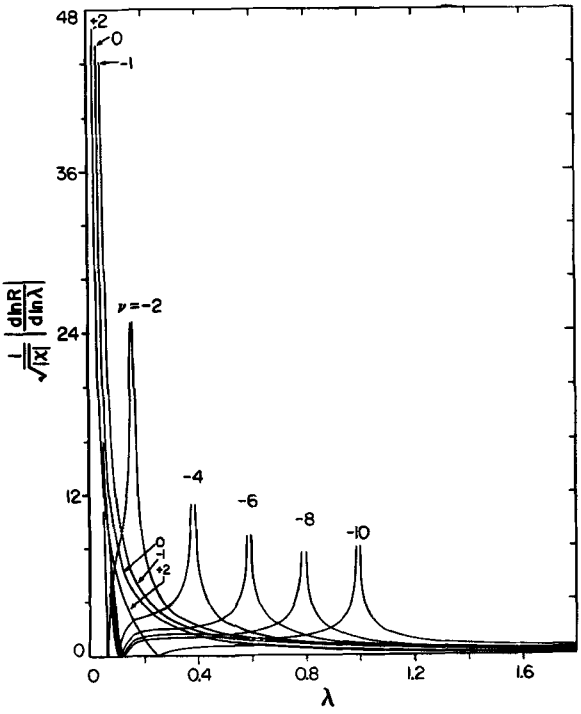

FIG. 10. The resolution factor, $(1/\sqrt{|\chi|})|d \ln R/d \ln \lambda|$, vs λ for different values of ν. These curves show the relative variation of resolution with λ (or molecular weight) with a constant flow $\langle v \rangle$.

factor $(1/\sqrt{\chi})|d \ln R/d \ln \lambda|$, which depends on the value of λ. This factor is plotted versus λ in Fig. 10 for different values of ν. In this figure $|\chi|$ is taken instead of χ to account for negative values below λ_{lim}.

Figure 10 shows that for values of ν smaller than -1, the resolution factor tends to infinity at a certain value of λ despite the fact that the opposing terms $|d \ln R/d \ln \lambda)|$ and $\sqrt{|\chi|}$ both tend to infinity. This can be shown by using Eq. (29):

$$\frac{1}{\sqrt{\chi}}\left|\frac{d \ln R}{d \ln \lambda}\right| = \frac{1}{\sqrt{\chi}}\left|\frac{dR}{d\lambda}\cdot\frac{\lambda}{R}\right| = \sqrt{\frac{1-e^{-1/\lambda}}{2F}}\left|\frac{dR}{d\lambda}\right|\frac{1}{\sqrt{R}} \tag{50}$$

When λ approaches λ_{lim}, R takes the form $k(\lambda - \lambda_{\text{lim}})$ as can be seen from Fig. 2, so that $dR/d\lambda$ becomes equal to k. In that case F tends to F_{lim}, a finite value, so that the terms depending on λ in the resolution expression

become

$$\lim_{\lambda \to \lambda_{\text{lim}}} \frac{1}{\sqrt{\chi}} \left| \frac{d \ln R}{d \ln \lambda} \right| = \sqrt{\frac{1 - e^{-1/\lambda_{\text{lim}}}}{2F_{\text{lim}}}} \sqrt{\frac{k}{\lambda - \lambda_{\text{lim}}}} \tag{51}$$

which shows that the resolution approaches infinity as λ approaches λ_{lim}. It is therefore possible by the proper adjustment of v to get high resolution for a specific range of λ values. This confirms our previous conclusions, based on selectivity considerations alone, that high resolution levels are possible in thermogravitational FFF for chosen values of λ and thus of molecular weight.

Unfortunately, as resolution tends to infinity, retention time t_r becomes very high and separation is correspondingly slow. If column length L in Eq. (49) is replaced by $t_R R\langle v \rangle$, we find the following square-root dependence of R_s on t_r:

$$R_s = \left[\frac{\gamma}{4} \sqrt{\frac{t_r D}{w^2}} \frac{\Delta M}{M} \right] \sqrt{\frac{R}{\chi}} \left| \frac{d \ln R}{d \ln \lambda} \right| \tag{52}$$

This equation can be used to predict changes in resolution with the time requirement fixed; that is, t_r = constant. The terms in the brackets are therefore again constant. The remaining factor, $K = \sqrt{R/\chi}\, |d \ln R/d \ln \lambda|$, is a function of λ. In Fig. 11 we plot curves for $K/K_0 = K(v)/K(v = 0) = R_s(v)/R_s(v = 0)$ versus v for different λ's. These curves simply represent the ratio of the resolutions obtained with thermogravitational FFF and normal (parabolic flow) FFF in a fixed time. The terminal points of the curves corresponding to $\lambda = 0.1$ to 0.5 correspond to the values of v for which $R = 0$. The sharp minima in relative resolution for positive values of v correspond to the points in Fig. 2 where the R versus λ curves have a maximum. At these maxima there is, of course, no differential migration and thus no resolution.

Figure 11 shows that for $\lambda \geq 0.5$ the thermogravitational FFF system shows a significant improvement in resolution in a fixed time for either upward or downward flow, depending on the magnitude of that time. For example, for $\lambda = 2$ the resolution is increased by a factor greater than 3 for $v < -0.6$ or $v > 1.4$. This means that it takes 3^2 (~ 10) times more time to get a given resolution with parabolic flow than with the vertical system.

Figures 10 and 11 are in basic agreement, showing that the potential of thermogravitational FFF lies in the fractionation of low molecular weight polymers (or of other components with weak thermal diffusion). As noted earlier, the pressurized thermal FFF system is aimed at the same

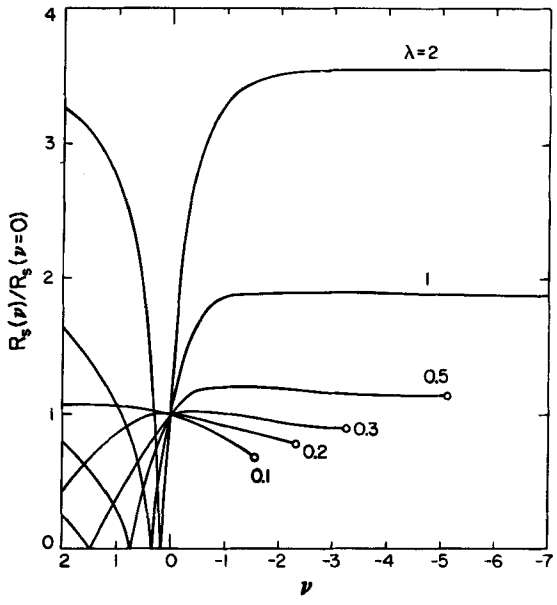

FIG. 11. Resolution relative to that for parabolic flow ($\nu = 0$) plotted against ν for different λ values.

class of materials. For the latter system a given increase in ΔT will decrease λ proportionally (Eq. 25). This will lead to an increase in resolution for a fixed time, or alternately an increase in speed for a fixed requirement on resolution (*9*). However, the two systems, pressurized and thermogravitational, are not incompatible, and it is likely that their combination will be beneficial in the separation of low molecular weight compounds.

Finally, we note that the conclusions drawn from Figs. 10 and 11 on the basis of Eqs. (48) to (52) are based on the assumption that the nonequilibrium factor provides the only significant contribution to the plate height. Experimental systems for which this is not true will require a different theoretical treatment. However, nonequilibrium-limited systems are the most efficient from a theoretical point of view, and thus ultimately from a practical point of view as well.

EXPERIMENTAL

The thermal FFF system used in this study was described in another paper (*9*). The channel was cut from a 0.127-mm thick Mylar sheet. Its effective length was 411 mm and its breadth 20 mm. Its volume was 1.095

ml. The system was turned on end to create thermogravitational conditions. Upward flow was used in these experiments.

All polymer samples but two were moderately dispersed polystyrene fractions ($\overline{M}_w/\overline{M}_n < 1.06$) supplied by Pressure Chemical Co. The exceptions were the 51,000 and 20,000 molecular weight polystyrenes of narrow polydispersity ($\overline{M}_w/\overline{M}_n \sim 1.009$) obtained from Waters Associates. The samples were introduced as 1 to 10 μl injections of 20 to 30 mg/ml of polystyrene in ethylbenzene solvent. No stop-flow procedure was used since it was calculated that the relaxation time for all polymers was about 10 sec (*3*).

In one group of experiments the temperature drop ΔT between the hot and cold walls was 40°C and the cold wall temperature was 18°C; in another group ΔT was 80°C and the cold wall was 22.5°C.

RESULTS AND DISCUSSION

We saw in the theoretical section that a change in the solvent flowrate in thermogravitational FFF will cause a variation in the relative importance of the forced and free convection terms which is reflected in coefficient v. It follows (see Eq. 16) that retention ratio R is a function of the imposed flow. This is illustrated in Fig. 12 where R for 110,000 molecular weight polystyrene is plotted against solvent velocity $\langle v \rangle$ for upward flow at $\Delta T = 40$°C and $T_c = 18$°C. We see that as $\langle v \rangle$ is reduced and v consequently becomes increasingly negative, R decreases as indicated in Eq. (16). The form of the variation of R with $\langle v \rangle$ for this experimental system involving upward flow can be compared with the theoretical curves for different λ values deduced from Eq. (16) and plotted in Fig. 13. (For completeness, the corresponding R versus velocity curves for downward flow are plotted in Fig. 14.)

Figure 13 shows that R should go to zero at a finite velocity. As the velocity approaches this critical value, R decreases sharply. Meaningful experimentation in this range requires a very accurate flow control. The experimental results of Fig. 12 show minimal scatter down to approximately half of the asymptotic R value, at which point the slope $dR/d\langle v \rangle$ is uncomfortably large. A further extension of the range toward $R = 0$ was deemed impractical. The experimental curve in Fig. 12 is similar to the plot corresponding to $\lambda = 0.10$ in Fig. 13. One can check the agreement between experimental data and the underlying expression, Eq. (16), by writing the latter as

$$v = \frac{R - R_p}{6\lambda(1 - R_p)} \tag{53}$$

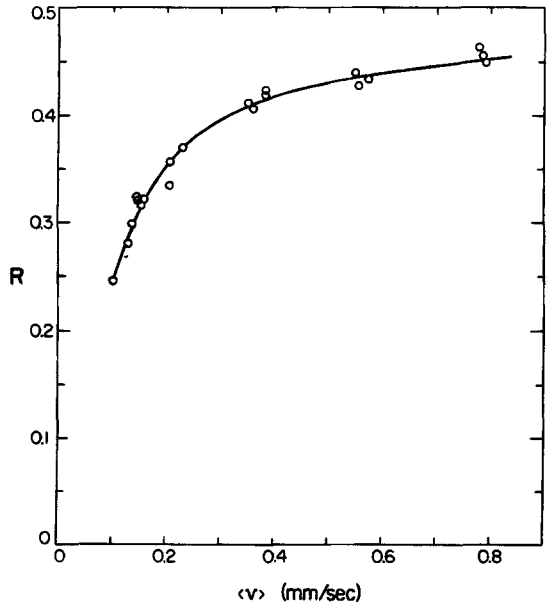

FIG. 12. Experimental R vs $\langle v \rangle$ plot for 110,000 molecular weight polystyrene in the thermogravitational FFF system with upward flow. Temperature conditions are $\Delta T = 40\,^{\circ}\mathrm{C}$ and $T_c = 18\,^{\circ}\mathrm{C}$.

If R_p and λ can be determined by measuring R, v can deduced. We stress that R_p cannot be taken as the retention ratio, R_{hor}, for horizontal systems. The difficulty is that the temperature dependence of viscosity distorts the flow profile of the horizontal system so that it is not parabolic. However, the distortion is such that the profile can be approximated by the third degree expression of Eq. (11) with v values ranging from 0 to about -0.5 (*24*). If we know R_{hor} and the corresponding v, v_{hor}, we can determine λ through Eq. (16) and then R_p through Eq. (17). For the vertical system, then, v in Eq. (53) represents the sum of v_{hor} and v_{vert}, the latter corresponding to the v value introduced solely by free convective flow. Values for v_{hor} can be calculated based on the temperature conditions of the system (temperature drop and cold wall temperature) and on the nature of the solvent. Since v_{hor}, R_p, and λ can all be determined, v_{vert} is determined from the retention ratio R_{vert} of the vertical system using

$$v_{vert} = [(R_{vert} - R_p)/6\lambda(1 - R_p)] - v_{hor} \tag{54}$$

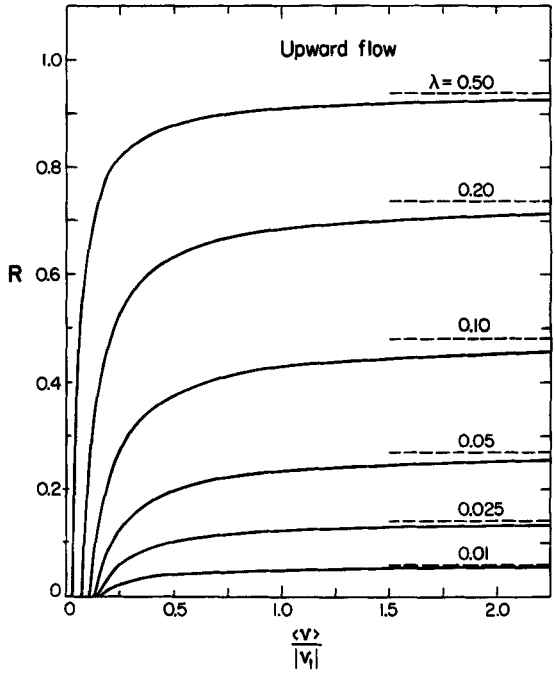

FIG. 13. Theoretical curve of R vs $\langle v\rangle/|v_1|$ in thermogravitational FFF with upward flow for different λ values. Asymptotic values shown at right.

From Eqs. (6) and (9), $v_{vert} = v_1/6\langle v\rangle$. This inverse dependence is tested in Fig. 15 where $-v_{vert}$ values calculated from Eq. (54) and the experimental data of Fig. 12 are plotted against $1/\langle v\rangle$. Parameters employed in this calculation are $v_{hor} = -0.149$, $R_p = 0.531$, and $\lambda = 0.1149$ ($R_{hor} = 0.483$). In spite of some scatter in Fig. 15, good agreement with the expected formation of a straight line is observed. A least-mean-squares analysis of the data gives the relationship

$$-v_{vert} = -0.02099 + 0.0810/\langle v\rangle \tag{55}$$

where $\langle v\rangle$ is in mm/sec. Although the correlation coefficient is 0.982, the intercept is slightly below zero. The small deviation might mean that the value, -0.149, taken for v_{hor} is somewhat too low (too high in absolute value). Nonetheless, the near-zero intercept and the linearity of the plot provide general support for the present treatment of retention despite the

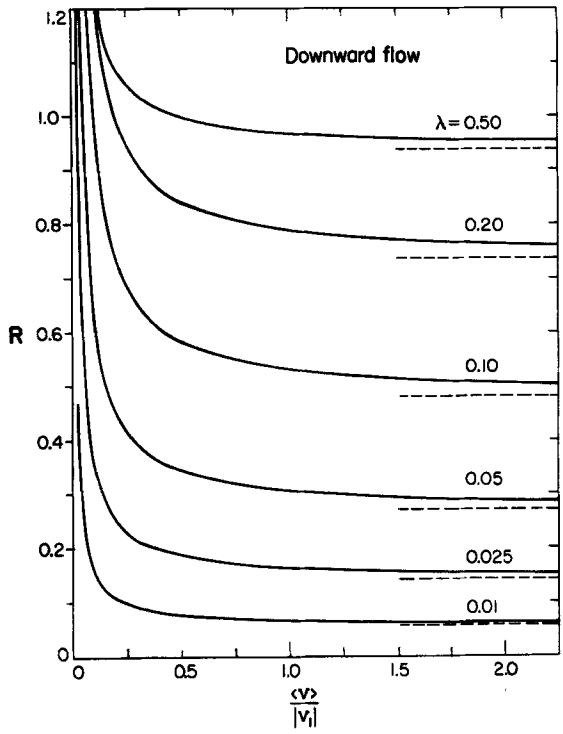

FIG. 14. Theoretical curves of R vs $\langle v \rangle / |v_1|$ with downward flow for different λ's.

neglect of the temperature dependence of viscosity for the free convective flow.

The slope of the line in Fig. 15, which should equal $|v_1/6|$ according to Eq. 10, yields $|v_1| = 0.4857$ mm/sec. This is considerably smaller than 0.941 mm/sec, the value calculated from Eq. (5) for ethylbenzene carrier and the parameters $\Delta T = 40°C$, $\gamma' = 1.1 \times 10^{-3}$ °C^{-1}, $w = 0.127$ mm, ρ (at 38°C, the center of the channel) = 0.850 g/cm^3 (*27*), and η (at 38°C) = 0.524×10^{-2} P (see Eq. 8 of Ref. 4) (*23*, *26*). Part of the difference may arise in uncertainty in the thermal expansion coefficient which is difficult to determine accurately.

The principal retention and flow characteristics for polymers of different molecular weights engaged in both horizontal and vertical flow are tabulated in Table 1. Two v_{vert} columns are given, the theoretical values

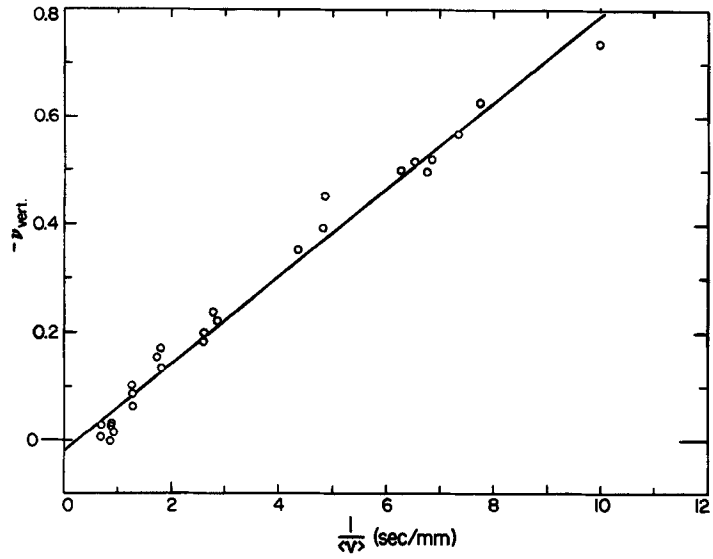

FIG. 15. Plot of $-v_{vert}$ values obtained from Eq. (55) and the experimental data of Fig. 12 vs $1/\langle v \rangle$.

TABLE 1

Retention and Flow Parameters for Polystyrene in Ethylbenzene Carrier with $\Delta T = 40°C$, $T_c = 18°C$, and $v_{hor} = -0.149$

Polymer molecular weight	R_{hor} (exp)	λ (calc)	R_p (calc)	R_{vert} (exp)	v_{vert} (theory)	v_{vert} (calc)	$\langle v \rangle$ (vert) (mm/sec)	$\lvert v_1 \rvert$ (calc) (mm/sec)
20,000	0.85	0.3497	0.886	0.657	−0.958	−0.809	0.102	0.495
37,000	0.71	0.2124	0.756	0.503	−0.814	−0.665	0.104	0.415
110,000	0.483	0.1149	0.531	0.245	−0.885	−0.736	0.100	0.441
160,000	0.41	0.0933	0.455	0.181	−0.898	−0.749	0.099	0.446

being those calculated from Eq. (16) using the stated R_{hor} and R_p values, and the calculated values being those due to free convection obtained by subtracting the contribution of v_{hor}. The dispersion in the listed v_{vert} values may stem partly from errors in the measurement of R, although some deviations arise because the velocity is not equal in all cases. The latter is shown by the fact that the standard deviation in the values of

TABLE 2

Retention and Flow Parameters for Polystyrene in Ethylbenzene Carrier with $\Delta T = 80°C$, $T_c = 22.5°C$, and $\nu_{hor} = -0.251$

Polymer molecular weight	R_{hor} (exp)	λ (calc)	R_p (calc)	R_{vert} (exp)	ν_{vert} (theory)	ν_{vert} (calc)	$\langle v \rangle$ (vert) (mm/sec)	$\lvert v_1 \rvert$ (calc) (mm/sec)
10,300	0.750	0.264	0.821	0.482	−1.195	−0.944	0.274	1.552
20,000	0.664	0.204	0.743	0.342	−1.275	−1.024	0.274	1.683
				0.414	−1.046	−0.795	0.345	1.646
37,000	0.474	0.123	0.556	0.167	−1.190	−0.939	0.274	1.544
				0.247	−0.945	−0.694	0.345	1.437
				0.260	−0.905	−0.654	0.362	1.420
				0.352	−0.624	−0.373	0.540	1.209
51,000	0.429	0.108	0.509	0.205	−0.953	−0.702	0.378	1.592
				0.306	−0.636	−0.385	0.547	1.264

$6\nu_{vert}\langle v \rangle = v_1$, shown in the last column of Table 1, is only 7.4%, which is less than that of ν_{vert}. Nevertheless, the average value, $|\bar{v}_1| = 0.449$ mm/sec, is well removed from the calculated one. Similar results were found for experiments with $\Delta T = 80°C$ and $T_c = 22.5°C$ ($\nu_H = -0.251$). The results are reported in Table 2. The average value is $|\bar{v}_1| = 1.48$ mm/sec with a standard deviation of 11.1%. As before, this is much smaller than the value of 2.32 mm/sec calculated from Eq. (5) using the appropriate parameter including ρ (at 62.5°C) = 0.828 g/cm^3 and η (at 62.5°C) = 0.414×10^{-2}.

The plate height curve obtained for vertical flow using 110,000 molecular weight polystyrene at $\Delta T = 40°C$ is plotted in Fig. 16. A least-mean-squares analysis of these data gives

$$H = 0.79 + 4.98\langle v \rangle \tag{56}$$

with a correlation coefficient of 0.961. Here $\langle v \rangle$ is in mm/sec and H in mm. We note that the intercept, 0.79 mm, is at the low end of the range, 0–4.0 mm, expected from the polydispersity contribution in the horizontal system assuming the supplier's polydispersity value of <1.06 (*28*). For the vertical system the upper limit of the range should in fact be higher since it is proportional to $(d \ln R/d \ln \lambda)^2$ (see Fig. 8).

The data of Fig. 16 tend to form a straight line much like that generally observed for horizontal systems, although there is no theoretical basis for this in the vertical system due to changing ν and χ values. It is likely that

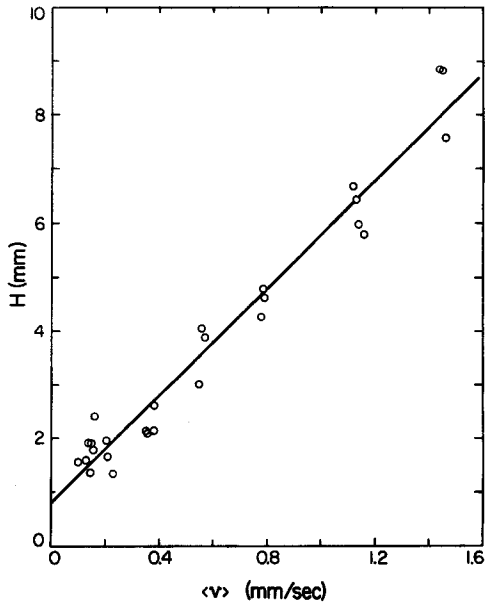

FIG. 16. Plate height data for 110,000 molecular weight polystyrene in vertical channel with upward flow. Least squares line is described by Eq. (56).

if the scatter in the data were reduced, the points would fit better to some nonlinear curve. It is interesting nonetheless that the slope of the line in Fig. 16, 4.98 sec, is only slightly higher than the slope expected for the horizontal configuration, 4.39 sec.

We note finally that several polystyrene polymer mixtures have been separated by the thermogravitational FFF system. Examples of the elution profiles are shown in Figs. 17 and 18. These separations were carried out with an 80°C temperature drop between walls, the colder of which was 22.5°C.

CONCLUSIONS

We have shown here that the thermogravitational FFF system behaves much as predicted by theory although there are several annoying discrepancies. We have also shown that it is possible to achieve polymer separations such as those shown in Figs. 17 and 18. While it might be possible, as noted in the theoretical section, to realize similar resolution with a

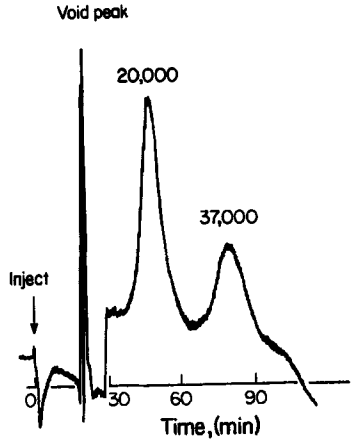

FIG. 17. Separation of linear polystyrenes of molecular weights 20,000 and 37,000 in thermogravitational FFF with upward flow. Conditions are $\Delta T = 80°C$, $T_c = 22.5°C$, flow rate = 3.04 ml/hr, $\langle v \rangle = 0.35$ mm/sec.

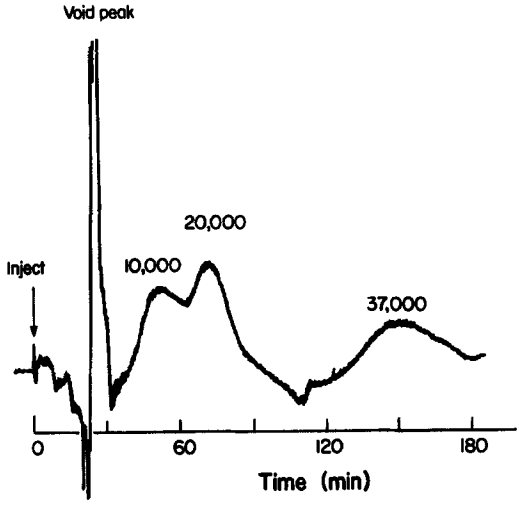

FIG. 18. Separation of three polystyrene fractions of molecular weights 10,300, 20,000, and 37,000 in thermogravitational FFF with upward flow. Conditions: $\Delta T = 80°C$, $T_c = 22.5°C$, flow rate = 2.42 ml/hr, $\langle v \rangle = 0.27$ mm/sec.

horizontal configuration, this could not be verified because of baseline problems at very low flow velocities.

The unique advantage of thermogravitational FFF is its presumed ability to maintain high resolution conditions into the low molecular weight range where horizontal systems offer little resolution. Indeed, since the retention of any species can be adjusted to zero by the proper setting of upward flow, it should be possible to begin a run at a velocity low enough to retain all but one of the components near the injection point, followed by gradual increases in flow which would elute or "desorb" successively higher molecular weight species of fractions. An alternate strategy for continuous or stepwise elution would be to maintain a fixed flow but gradually rotate the column from a vertical to a horizontal position. We note also that one could achieve similar ends by using programmed changes in the temperature drop between walls, a technique already used to great advantage with horizontal columns (*7*).

Unique effects could also be realized with changes in column geometry. A tapered channel in which either width or breadth increased with height would lead to the formation of stationary zones which could be gradually bled from the system as discrete fractions.

Clearly the thermogravitational FFF system provides a number of new options for polymer separations. The increased control of flow near the cold wall leads to the direct control of polymer migration and differentiation, and makes several new programming systems possible. In addition, improved retention and resolution are anticipated for low molecular weight materials. While this paper has barely touched on these new approaches, it has established a theoretical framework by which results can be predicted and systems optimized. Hopefully this will aid in the development of practical techniques based on thermogravitational FFF at some time in the future.

Acknowledgment

This investigation was supported by National Science Foundation Grant No. CHE76–20870.

SYMBOLS

A	Rayleigh number
c	local concentration of solute
c_p	specific heat at constant pressure

D	solute–solvent diffusion coefficient
F	term defined by Eq. (30)
g	gravitational acceleration
H_D	longitudinal molecular diffusion contribution to plate height
H_N	nonequilibrium contribution to plate height
H	plate height
K	$\sqrt{R/\chi}\,\lvert d \ln R/d \ln \lambda\rvert$
k	defined by limiting form $R = k(\lambda - \lambda_{\text{lim}})$
L	channel length
M	molecular weight of solute
N	number of theoretical plates
R	retention ratio
R_{hor}	retention ratio for horizontal systems
R_{vert}	retention ratio for vertical systems
R_p	retention ratio due to parabolic flow
R_s	resolution of two components
t_r	retention time
v_{free}	velocity profile due to convective flow
v_{forced}	velocity profile due to forced flow
$\langle v \rangle$	average solvent velocity
V_r	retention volume
V^0	void volume
w	channel thickness, the distance between the hot and cold walls
x	distance from cold wall
ℓ	mean "thickness" of solute layer
$\mathscr{V}$	mean solute velocity
$\mathscr{L}(y)$	Langevin function defined by Eq. (18)
α	thermal diffusion factor of solute
χ	nonequilibrium coefficient defined by Eq. (26)
ΔT	temperature difference between the hot and cold walls
η	viscosity of the solvent
γ'	coefficient of thermal expansion
γ	$\lvert d \ln \lambda/d \ln M\rvert$
κ	thermal diffusivity
λ	ℓ/w, dimensionless layer thickness
λ'	thermal conductivity
ν	flow parameter defined by Eq. (9)
ν_{hor}	ν for horizontal system
ν_{vert}	ν for vertical system

ϕ parameter defined by Eq. (25)
ρ density of the solvent
ψ nonequilibrium coefficient defined by Eq. (27)
θ parameter defined by Eq. (45)

REFERENCES

1. J. C. Giddings, *Sep. Sci.*, *1*, 123 (1966).
2. J. C. Giddings, *J. Chem. Educ.*, *50*, 667 (1973).
3. M. E. Hovingh, G. H. Thompson, and J. C. Giddings, *Anal. Chem.*, *42*, 195 (1970).
4. M. N. Myers, K. D. Caldwell, and J. C. Giddings, *Sep. Sci.*, *9*, 47 (1974).
5. J. C. Giddings, Y. H. Yoon, and M. N. Myers, *Anal. Chem.*, *47*, 126 (1975).
6. J. C. Giddings, L. K. Smith, and M. N. Myers, *Ibid.*, *47*, 2389 (1975).
7. J. C. Giddings, L. K. Smith, and M. N. Myers, *Ibid.*, *48*, 1587 (1976).
8. L. K. Smith, M. N. Myers, and J. C. Giddings, *Ibid.*, *49*, 1750 (1977).
9. J. C. Giddings, M. Martin, and M. N. Myers, *J. Chromatogr.*, *158*, 419 (1978).
10. K. Clusius and G. Dickel, *Naturwissenschaften*, *26*, 546 (1938).
11. P. E. Grodzka and B. Facemire, *Sep. Sci.*, *12*, 103 (1977).
12. J. W. Elder, *J. Fluid Mech.*, *23*, 77 (1965).
13. E. R. G. Eckert and W. O. Carlson, *Int. J. Heat Mass Transfer*, *2*, 106 (1961).
14. R. C. Reid, J. M. Prausnitz, and T. K. Sherwood, *The Properties of Gases and Liquid*, 3rd ed., McGraw-Hill, New York, 1977.
15. P. Debye, *Ann. Phys.* (*5*), *36*, 284 (1939).
16. R. C. Jones and W. H. Furry, *Rev. Mod. Phys.*, *18*, 151 (1946).
17. J. W. Hiby and K. Wirtz, *Phys. Z.*, *41*, 77 (1940).
18. S. R. DeGroot, *Physica*, *9*, 801 (1942).
19. P. Debye and A. M. Bueche, *High Polymer Physics*, Chemical Publishing Co., New York, 1948, p. 497.
20. R. B. Bird, W. E. Stewart, and E. N. Lightfoot, *Transport Phenomena*, Wiley, New York, 1960, p. 297.
21. W. Jost, *Diffusion in Solids, Liquids, and Gases*, Academic, New York, 1960, p. 510.
22. S. R. DeGroot, *L'effet Soret*, North Holland, Amsterdam, 1943.
23. J. C. Giddings, K. D. Caldwell, and M. N. Myers, *Macromolecules*, *9*, 106 (1976).
24. K. D. Caldwell, M. Martin, and J. C. Giddings, *Sep. Sci. Technol.*, To Be Published.
25. M. Martin and J. C. Giddings, *J. Phys. Chem.*, Submitted.
26. J. K. Horrocks and E. McLaughlin, *Trans. Faraday Soc.*, *59*, 1709 (1963).
27. *Handbook of Physics and Chemistry* (R. C. Weast, ed.), 52nd ed., Chemical Rubber Co., Cleveland, 1971–72.
28. M. Martin, M. N. Myers, and J. C. Giddings, *J. Liq. Chromatogr.*, Accepted.

Received by editor November 27, 1978